Journal of Structural Geology 32 (2010) 1742–1753

Contents lists available at ScienceDirect

Journal of Structural Geology

journal homepage: www.elsevier.com/locate/jsg

Simulating brittle fault evolution from networks of pre-existing joints within crystalline rock

Heather Moir [a,*], Rebecca J. Lunn [a], Zoe K. Shipton [b], James D. Kirkpatrick [b]

[a] Department of Civil Engineering, University of Strathclyde, Glasgow, Scotland, UK
[b] Department of Geographical and Earth Sciences, University of Glasgow, Glasgow, Scotland, UK

ARTICLE INFO

Article history:
Received 9 February 2009
Received in revised form
17 August 2009
Accepted 20 August 2009
Available online 23 September 2009

Keywords:
Numerical modelling
Fault-zone evolution

ABSTRACT

Many faults grow by linkage of smaller structures, and damage zones around faults may arise as a result of this linkage process. In this paper we present the first numerical simulations of the temporal and spatial evolution of fault linkage structures from more than 20 pre-existing joints, the initial positions of which are based on field observation. We show how the constantly evolving geometry and local stress field within this network of joints contribute to the fracture pattern. Markedly different fault-zone trace geometries are predicted when the joints are at different angles to the maximum compressive far-field stress ranging from evolving smooth linear structures to complex 'stepped' fault-zone trace geometries. We show that evolution of the complex fault-zone geometry is governed by: (1) the strong local variations in the stress field due to complex interactions between neighbouring joints; and (2) the orientation of the initial joint pattern with respect to the far-field stress.

1. Introduction

Several authors have proposed that faults evolve under imposed stress by the linkage of pre-existing structures (Segall and Pollard, 1983; Martel, 1990; Bergbauer and Martel, 1999; Pachell et al., 2003). The pre-existing structures from which faults nucleate are commonly open or mineral-filled joints that are weaker than the surrounding rock (Segall and Pollard, 1983; Bergbauer and Martel, 1999; Pachell and Evans, 2002). When pre-existing features experience compressive loading, stress concentrations (both tensile and shear) develop around the tip of the feature. Shearing of these pre-existing features often results in the formation of secondary fractures at (or near) the tip of the feature. These secondary fractures have different names including: tail cracks/fractures (Cruikshank and Aydin, 1994; Willemse et al., 1997), splay fractures (Pachell and Evans, 2002; Myers and Aydin, 2004), horsetail fractures (Granier, 1985; Kim et al., 2004) and wing cracks (Crider and Peacock, 2004). In this paper all fractures (tension or shear) associated with faulting at (or near) the tip of a pre-existing feature are termed wing cracks. Conceptual models of fault evolution through the development of wing cracks (Martel, 1990; Martel and Boger, 1998) are supported by field observations of wing crack evolution from single joints or faults (Kattenhorn and Marshall, 2006; Joussineau et al., 2007) and by observations of linking fractures that have developed between pairs of isolated faults (Peacock and Sanderson, 1995; Kim et al., 2004). Wing cracks developing with shear displacement are also commonly observed in field data, for instance the sheared dyke in Fig. 1a and the large splay faults in Kirkpatrick et al. (2008, their Fig. 8).

In this paper, we focus on fault-zone development in crystalline rocks. Natural exposures of fault-zone traces within crystalline rocks can have many geometries, from smooth, approximately planar features (Fig. 1a) where faults appear to develop along strike, to complex stepped structures (Fig. 1b) where adjacent faults are linked at stepovers, or a combination of both (Fig. 1c). Key questions are: what governs the geometry of the evolving fault-zones? How are fractures within the fault-zone linked?

A series of numerical models simulating fault growth, support these conceptual models for fault-zone evolution. These models have simulated the evolution of wing cracks from the tips of pre-existing structures (Shen and Stephansson, 1993; Bürgmann et al., 1994; Kattenhorn et al., 2000; Willson et al., 2007) or the linkage of pairs of faults with extensional and contractional geometries (Du and Aydin, 1995; Bremaecker and Ferris, 2004; Lunn et al., 2008). These simple, two-dimensional (2D) models have enabled prediction of the orientation of linkage fractures and their mode of failure, for a single fracture or pair of fractures in an ideal homogeneous medium. However, these simulations, derived from one or two fractures, are not sufficient to understand the range of complex geometries observed in the field (Fig. 1). Within this paper we

* Corresponding author at: Department of Civil Engineering, University of Strathclyde, 16 Richmond Street, Glasgow G1 1XQ, Scotland, UK.
E-mail address: heather.moir@strath.ac.uk (H. Moir).

0191-8141/$ – see front matter © 2009 Elsevier Ltd. All rights reserved.
doi:10.1016/j.jsg.2009.08.016

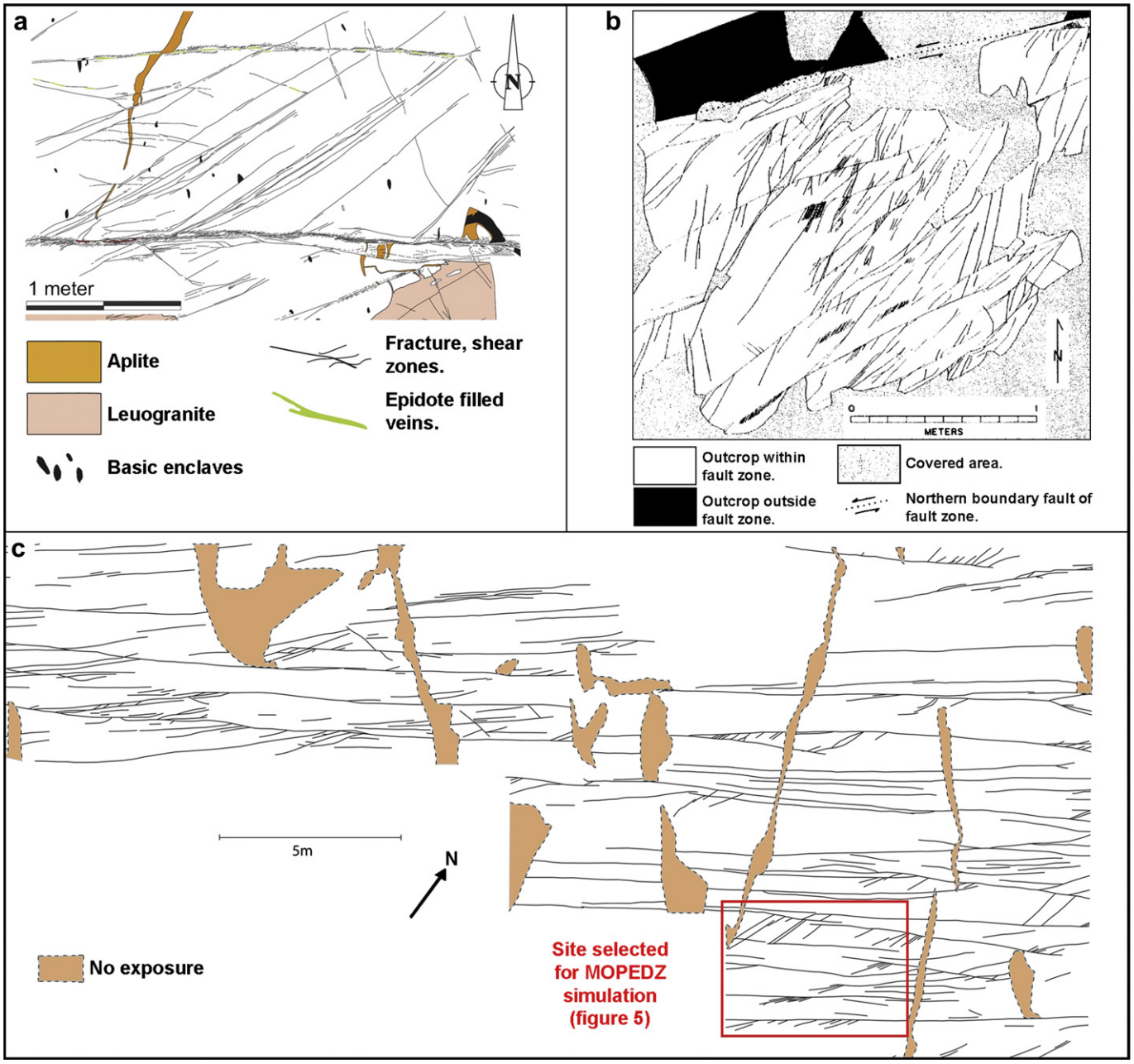

Fig. 1. Field examples of mapped sections from fault-zones. (a) A segment of the outcrop map from NE of Neves lake in the Italian Alps showing a section of fault-zone with smooth planar features (Pennacchioni and Mancktelow, 2007). (b) A segment of the outcrop map from the Waterfall region in the Sierra Nevada, California (Martel, 1990). (c) Map of fractures in an exposure of the Lake Edison granodiorite in the Bear Creek region in the Sierra Nevada, California, UTM coordinates are: 0333075 4136569.

extend current knowledge by simulating fault-zone evolution in granite from a network of more than 20 joints. We show that evolution of the resulting fault-zone geometry is governed by: (1) the strong local variations in the stress field due to complex interactions between neighbouring joints; and (2) the orientation of the initial joint pattern with respect to the far-field stress.

2. Methodology

We use the computer code Modelling Of Permeability Evolution in the Damage Zone surrounding faults (MOPEDZ) (Willson et al., 2007) to simulate spatial and temporal evolution of complex patterns of linking fractures. MOPEDZ was developed using the commercially available finite-element software COMSOL which is called from within the MATLAB code. The COMSOL finite-element routines assume plane strain during the simulations. MOPEDZ is a 2D finite-element model which solves Navier's equation in a series of 'quasi' steady-states and uses a combined Mohr Coulomb and tensile failure criteria. Elements within the finite-element mesh are either intact host rock or fractured host rock. Elements which contain fractures (including the initial joints) are represented by lower effective material values (10% of the host) for Young's modulus, Poisson's ratio and material strength, in a similar approach to Tang (1997). Representing the accumulation of damage within each element by altering that element's material properties is consistent with other damage mechanics models (Jing, 2003).

The initial configuration for all MOPEDZ simulations is similar to that illustrated in Fig. 2 with the host rock (granodiorite) having the

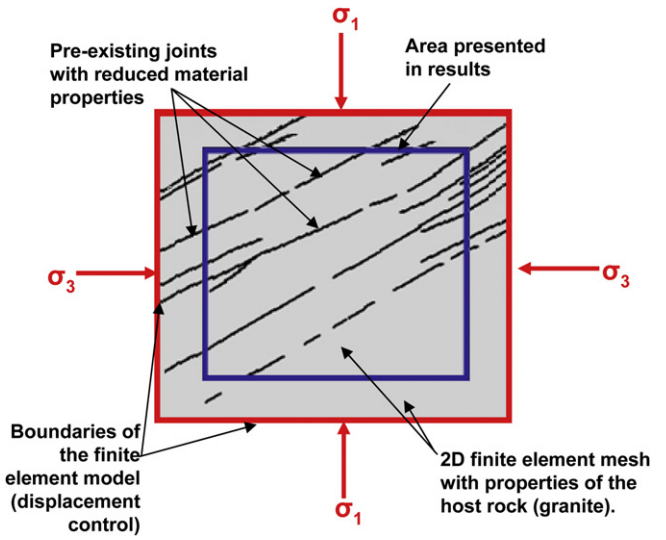

Fig. 2. Typical initial setup showing the orientation of σ_1 and σ_3 (simulated far-field stress). Gray area is host rock, black is host rock containing joints (n.b. the pixellated nature of the pre-existing joints is a product of the model). The model boundaries (red) are under displacement control, following the initial failure only the top and bottom boundaries are displaced. To avoid consideration of structures generated at the boundary in the large simulations, only the central window (within the blue box) was presented in the results. For all small simulations no window was taken and all results within the red model boundaries are presented. The number of mesh elements varies from 6400 to 136,500 depending on the size of the simulation. (For interpretation of the references to colour in this figure legend, the reader is referred to the web version of this article.)

properties listed in Table 1 and any elements containing pre-existing joints having reduced material properties (10% of the host) (Willson et al., 2007). The simulated maximum compressive far-field stress direction, σ_1, is parallel to the y axis (i.e. top-to-bottom in all MOPEDZ figures) and the minimum, σ_3, is parallel to the x axis (i.e. left-to-right in all MOPEDZ figures) (Fig. 2). Note that in the field both σ_1 and σ_3 are horizontal. Initially all boundaries are displaced inward holding $\sigma_1 = 2\sigma_3$, (in compression) however following the first failure (either Mohr Coulomb or tensile) the σ_3 boundaries are held constant and from this point on only the σ_1 boundaries are displaced towards each other, i.e. σ_1 progressively increasing with σ_3 held constant. All simulations presented here are in compression. Throughout this paper σ_1 and σ_3 refer to the far-field stress imposed by the boundaries of the finite-element model and σ_1^{Local} and σ_3^{Local} refer to the local stress field around damaged cells. All simulations use square finite-elements; the number of mesh elements in the simulations presented in this paper varies from 6400 to 136,500; the size of each cell is approximately 13 mm^2.

Table 1
MOPEDZ simulation parameters for brittle rock.

Rock property	Value	Reference
Host Rock Young's modulus	60 GPa	Martin (1997) Turcotte and Schubert (2002)
Host rock Poisson's ratio	0.2	Turcotte and Schubert (2002)
Young's modulus of fractured element	1.2 GPa	Segall and Pollard (1983)
Poisson's ratio of fractured element	0.02	
Co (shear strength)	130 MPa	Martin (1997)
μ (coefficient of friction)	0.6	Byerlee (1967)
To (tensile strength)	10 MPa	Martin (1997)
Number of cells permitted to fail in any one step of the MOPEDZ code	6	

Where relevant the right hand column contains the reference from which the value of the mechanical property was derived.

As an element fails (in either shear or tension) its material properties are altered. Although the first failures are triggered by displacement of the boundaries, the alteration of the material properties of those failed cells causes a change in both the direction and magnitude of σ_1^{Local} and σ_3^{Local} (Lunn et al., 2008). This alteration of the local stress may be sufficient to trigger additional failures without any further displacement of the model boundaries. These subsequent failures can be adjacent to previous failures, i.e. representing the lengthening of a macroscopic fracture, or they can occur in locations that are disconnected from any previous failure, or they may be further fracturing of the same element or any combination of these. MOPEDZ iteratively reduces the values of the material properties as elements are predicted to fail; this reflects increasing damage to the host rock (host rock elements containing pre-existing joints start with the lowest values, 10% of host rock). Each element can fail up to a maximum of six times (resulting in a reduction of strength, Young's modulus and Poisson's ratio) in a geometric sequence (Willson et al., 2007) until they reach the lowest value permitted (equivalent to those elements containing the initial joints). We emphasise that each element in the mesh may represent, at a sub-element scale, any number of micro or macroscopic failures in the field (in these simulations a sub-element scale is smaller than 13 mm^2).

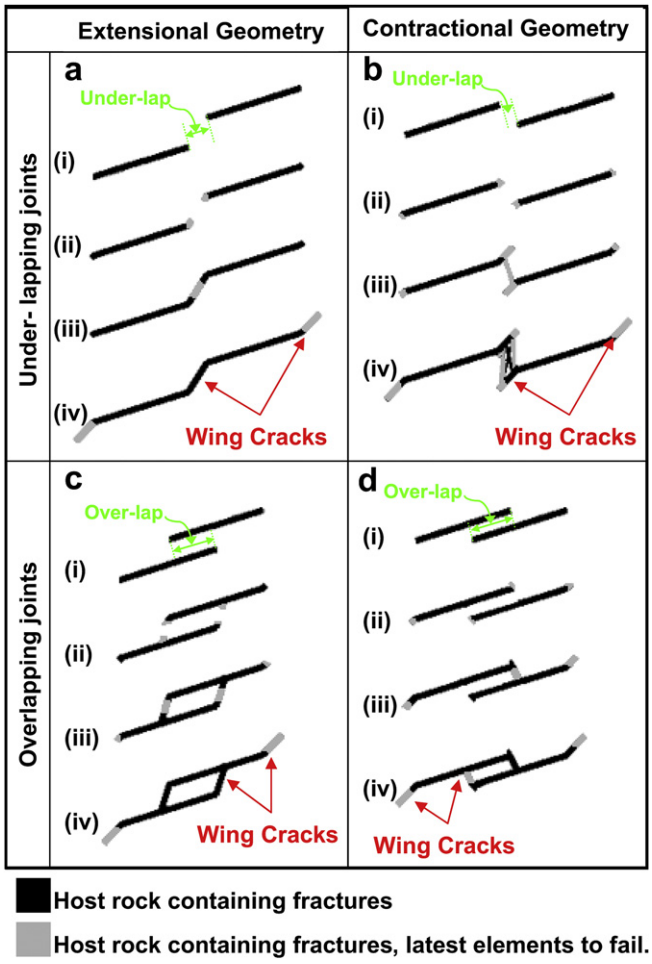

Fig. 3. Cartoon showing the evolution of restraining and releasing bends for a pair of overlapping and under-lapping pre-existing joints with either contractional or extensional relationship, (i) is the initial orientation of the joints, and sequences (ii–iv) show evolution of the predicted structure. All slipped joints are left lateral.

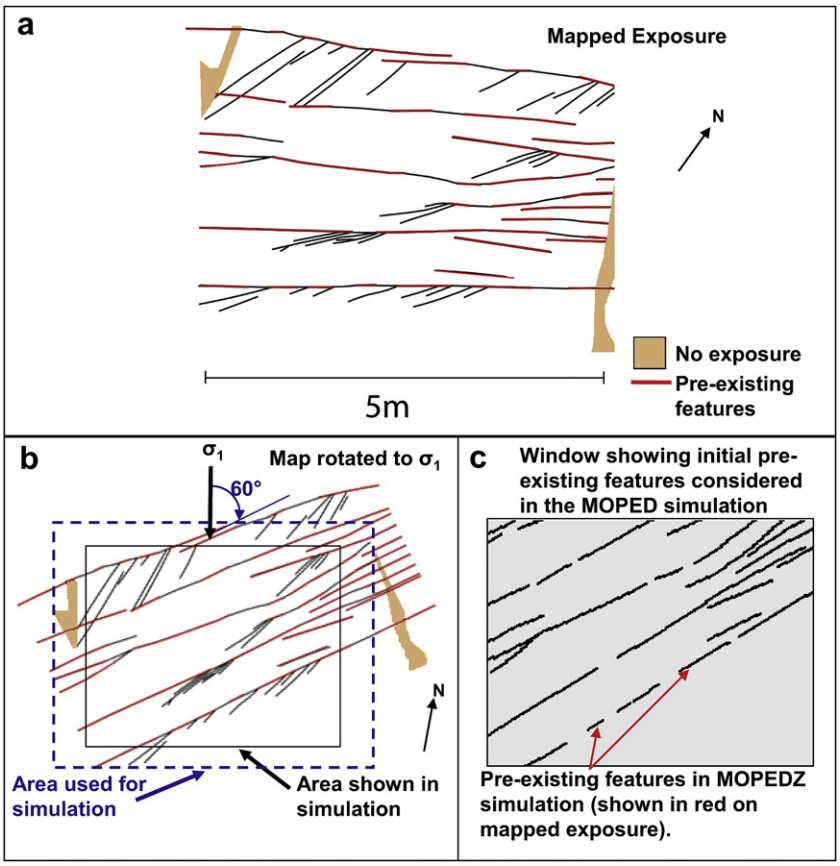

Fig. 4. (a) Small section from map shown in Fig. 1c. (b) Mapped joints oriented at 60° to the maximum principal stress (σ_1) (model requires σ_1 to be parallel to the *y* axis). (c) Finite-element mesh containing initial pre-existing joints (n.b. the pixelated nature of the pre-existing joints is a product of the model).

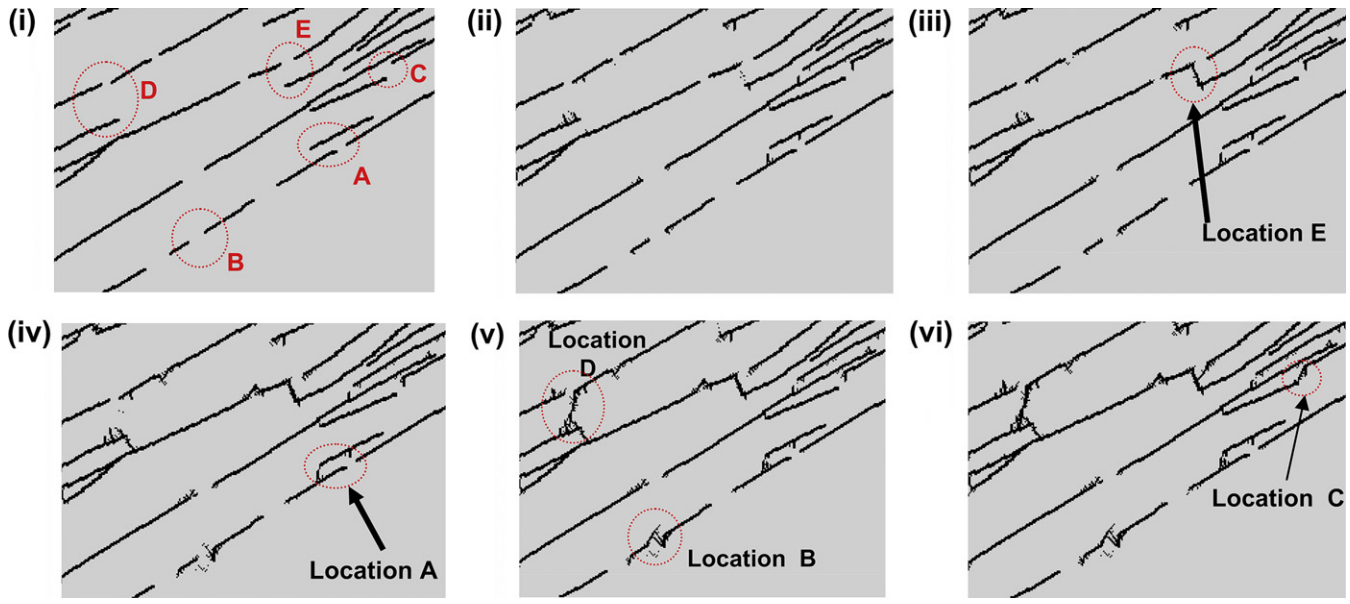

Fig. 5. Damage plot showing six frames from a simulation consisting of 350 steps which illustrate the temporal evolution of the linking fractures predicted by MOPEDZ from (i) the initial joints through to (vi) the final structure (finite-element mesh 390 × 350). The joints are oriented at approximately 60° to σ_1. Linkages at Location A are in a different orientation to the rest of the simulation (see Fig. 7). At Location B overlapping joints in an extensional geometry link in a similar way as those in Fig. 3c. At Location C under-lapping joints in a contractional geometry link in a similar way as those shown in Fig. 3b. At Location D two closely spaced joints in a contractional geometry link with a third more distant joint which is in an extensional geometry. At Location E joints under-lapping and in an extensional geometry link in a similar way as those shown in Fig. 3a. All slipped joints are left lateral.

Once a steady-state solution has been achieved for a given boundary displacement, the top and bottom boundaries undergo further displacement towards each other and the whole solution process is repeated. During any one iteration of the code, only a small number of elements (<6 in these simulations) are permitted to fail to ensure stability of the model solution and provide an estimation of the temporal propagation of the fractures.

Earlier research using MOPEDZ to examine failure from a single joint (Willson et al., 2007) shows that fracture-trace geometries are not sensitive to the initial mechanical properties of the host rock (Table 1), e.g. if Young's modulus of the crystalline host rock is lower, the same trace geometries are formed but at lower values of the displacement of the boundaries. Fracture-trace geometries are principally determined by local variations in the Young's modulus (i.e. damaged elements), the orientation of the pre-existing joint to the far-field maximum compressive stress and the ratio of σ_1–σ_3. In simulations where $\sigma_1 \gg \sigma_3$, failure was predominately in tension, for those where σ_1 is close to $2\sigma_3$, simulated failure was predominately in shear. The mode of failure results in different orientations of the evolving linkage fractures (Lunn et al., 2008). MOPEDZ simulations of fault linkage involving just two initial joints (Lunn et al., 2008) showed that fracture-geometries develop in a predictable way summarised in Fig. 3. Four initial stepover geometries were modelled: (a) under-lapping extensional; (b) under-lapping contractional; (c) overlapping extensional; and (d) overlapping contractional. The geometries of linkage structures are governed by three key factors: (1) the ratio of σ_1–σ_3; (2) the initial relative positions of the joints, specifically, contractional vs. extensional geometries and overlapping vs. under-lapping joints; and (3) the orientation of the most compressive principal stress direction (σ_1) relative to the initial pair of joints.

In the following simulations we explore fault-zone evolution through a large population of over 20 initial joints with gradually increasing displacement of the σ_1 boundaries of the model while σ_3 boundaries are held constant. We start from an initial condition for

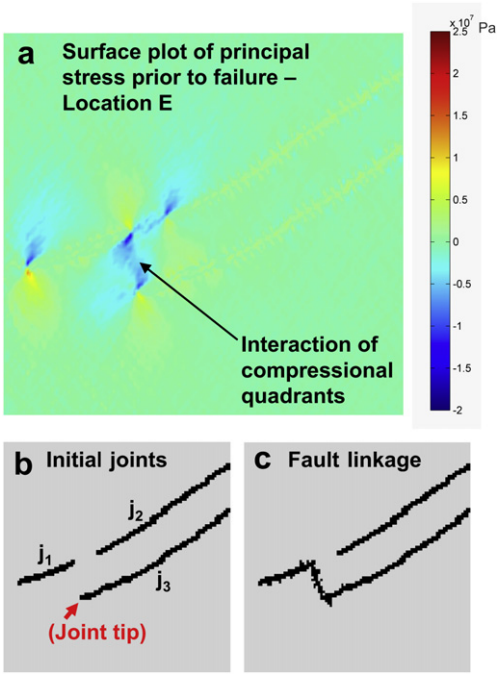

Fig. 6. Small simulation (80 × 80 finite-element mesh) with the joints in the same orientation as Location E. (a) Surface plot of the principal stress prior to failure showing interaction of the compressional quadrants of both joints. (b) Initial joint pattern entered into MOPEDZ (overlap between j_1 and j_3 of 38 mm). (c) Damage plot of the final structure obtained.

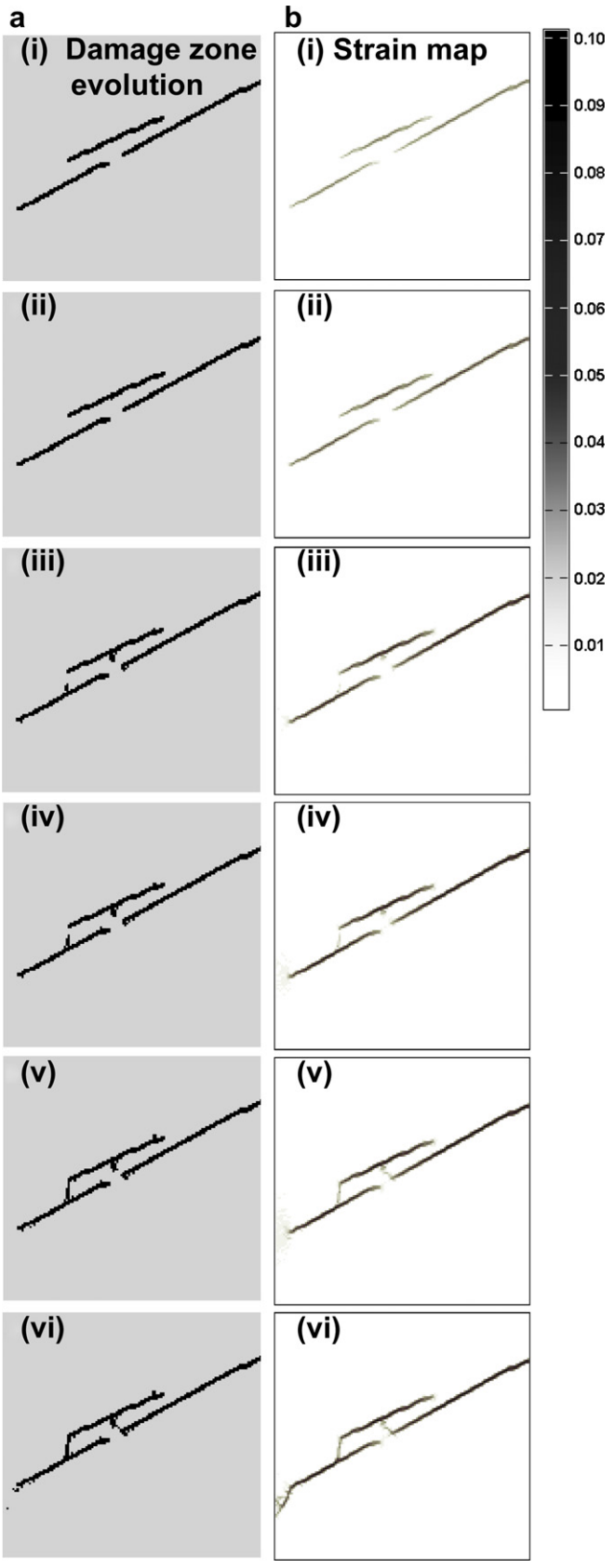

Fig. 7. Small simulation with joints in the same orientation as Location A. (a) The spatial and temporal evolution of the linking fractures predicted by MOPEDZ; black represents elements of the of the finite-element mesh which contains fractures. (b) Plots of the norm of the strain tensor which give a scalar representation of the magnitude of the strain tensors; the darker the colour the higher the strain.

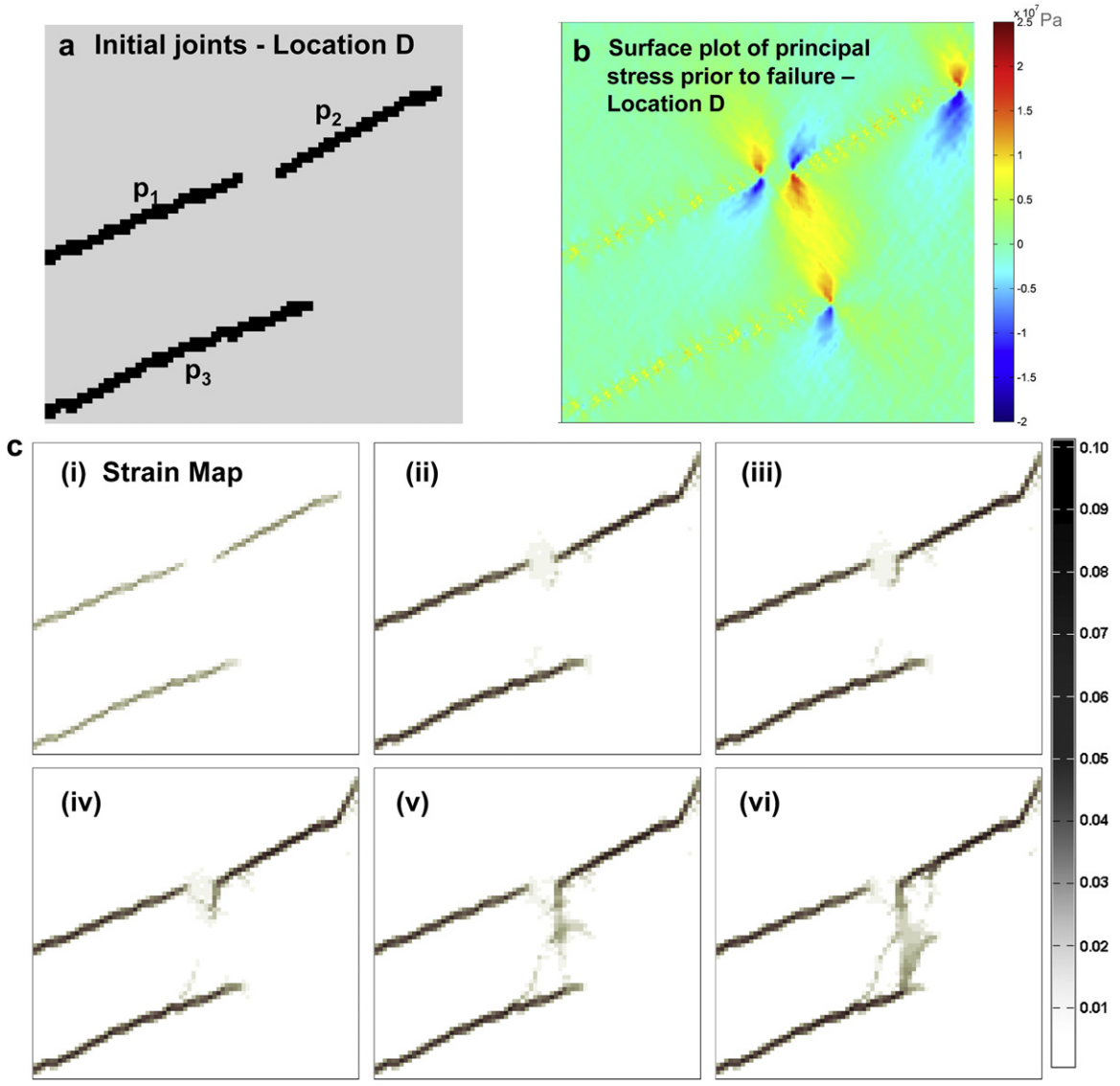

Fig. 8. Small simulation with joints in the same orientation as at Location D. (a) Initial orientation of joints for MOPEDZ simulation (80 × 80 finite-element mesh, the pixelated nature of the pre-existing joints is a product of the model). (b) Surface plot of the principal stress immediately prior to first failure. (c) Plots of the norm of the strain tensor (scalar representation of the magnitude of the strain tensors) illustrating the predicted evolution of the fractures.

far-field stresses of $\sigma_1 = 2\sigma_3$. Within the initial joint population, all four configurations of joint stepovers (as seen in Fig. 3) are locally present. The simulations are conducted with the joints at two angles to σ_1 (approximately 60° and 30° to the initial joints). To explore the effect of local stress perturbations within a *large* joint network (>20 joints), simulation results are compared to the linkage structures predicted for pairs of joints illustrated in Fig. 3.

2.1. Specifying the location and orientation of the pre-existing joints

The distribution of the pre-existing joints for the following MOPEDZ simulations are based on part of an exposure of the Lake Edison granodiorite in the Mount Abbot Quadrangle in the central Sierra Nevada, California (Figs. 1c and 4a). Martel (1990), Evans et al. (2000) and Kirkpatrick et al. (2008) show that faults in granites in the Sierra Nevada have fault cores defined by zones of cataclasite and ultracataclasite and damage zones consisting of joints and minor faults. These faults are thought to have developed through slip along a population of joints (Segall and Pollard, 1983). These joints were most likely formed during the cooling of the plutons (Bergbauer and Martel, 1999). Observations suggest that slip along the joints was accompanied by the development of wing cracks and linkage structures forming small fault-zones (Martel et al., 1988). Field observations were used to approximate the sections of the small faults that may have comprised the original joints (before some joints were reactivated). Un-reactivated joints were identified as fractures that exhibit zero shear offset (through observations of aplite dykes or mafic enclaves) and lack any association with wing cracks. The locations of reactivated joints were then defined as those portions of the small faults that have similar trace orientations (within 10°) to the un-reactivated joints. The initial joint population input into the following MOPEDZ simulations includes both the un-reactivated and reactivated joints. We emphasise that the purpose of the following simulations is not to reproduce the detailed fault trace geometries observed in the field (since the actual locations of original joints are not known) but to investigate conditions that may promote differing styles of fault-zone development.

The initial joint pattern that was input into MOPEDZ and its relationship to the fracture-traces mapped in the field is shown in Figs. 4a–c. With the exception of the final simulation the joints are at

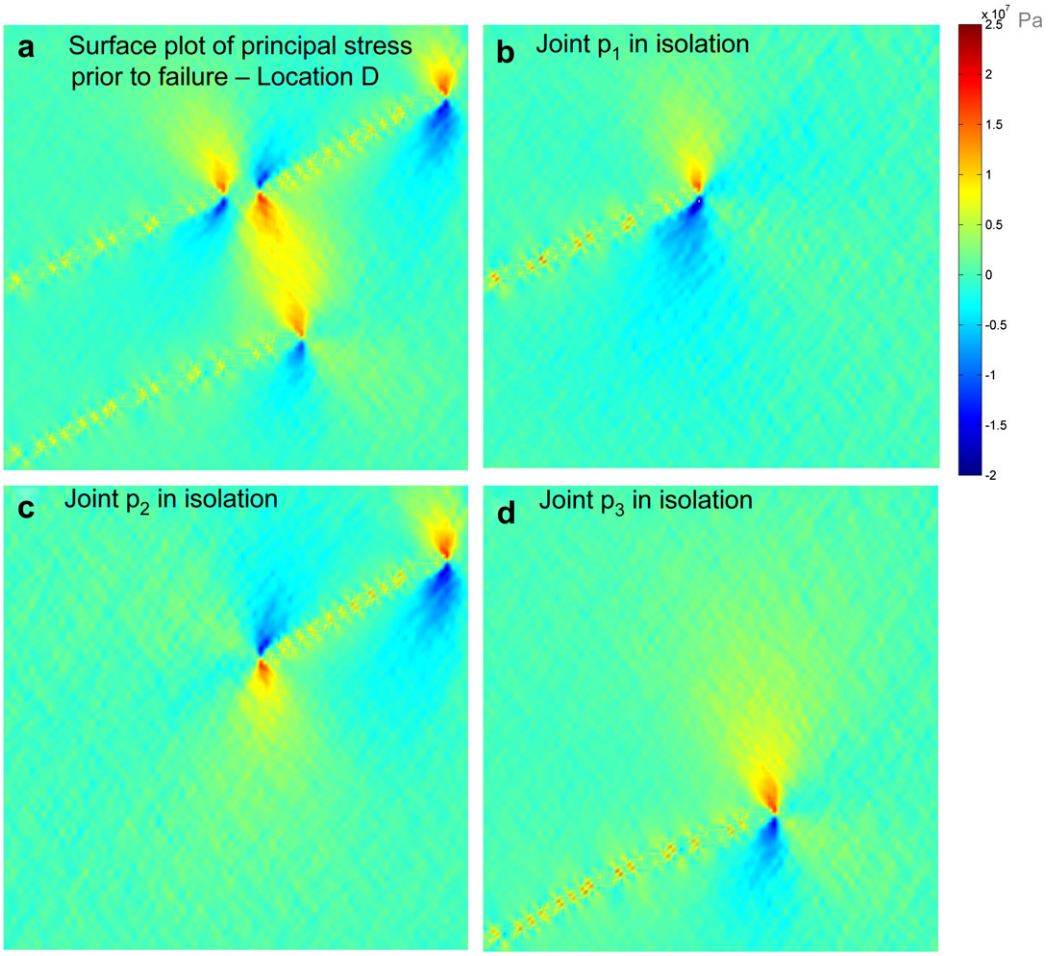

Fig. 9. Surface plot of the principal stress prior to failure for individual pre-existing structures in the same orientation as those at Location D, Fig. 5.

approximately 60° to σ_1. Stress around pre-existing joints which intersect the boundaries may be influenced by the proximity of the boundary. For the simulations with >20 joints, to avoid consideration of any structures which might result from boundary effects, results are displayed and discussed only for an internal area in the centre of the finite-element mesh, the edges of which are defined in Fig. 4b. Small-scale simulations are also presented, to investigate behaviour at specific locations within the larger mesh. These smaller scale simulations display results over the whole model domain (i.e. no window is taken). In each case, initial damage predictions for the small mesh were compared with those within the larger mesh to confirm that predicted structures were similar, and hence that boundary conditions were not having a substantial effect on model results.

2.2. Presentation of simulation results

Simulation results are illustrated using three types of maps. (1) Damage plots show the elements that have failed – grey indicates intact host rock and black indicates fractured host rock (since individual elements may fail multiple times in shear and/or tension, modes of failure are not shown). (2) Strain plots show the Euclidean norm of the strain tensor, which is one of the methods of representing the scalar magnitude of a strain tensor (Mathews and Fink, 2004). Plots of the norm of the strain tensors for each element elucidate a more detailed structure than the damage plots, since they also highlight elements which are under a high strain but that have not yet failed. The norm of the strain tensor presented here may not be appropriate for direct comparison with field data since we start all simulations from an initial condition of zero strain. (3) Surface plots of the local principal stress show the spatial distribution of σ_1^{Local}; these plots have the same colour scale to allow easy comparison between simulations. Note that surface plots of the local principal stress were produced within COMSOL in which compression is negative and tension positive (the opposite convention is usually adopted within the geological literature).

3. Results

3.1. Development of linkage structures

The spatial and temporal evolution of the fracture development and linkage predicted by MOPEDZ, for the joint pattern in Fig. 4c, is shown in Fig. 5 as a damage plot. The initial joints are at approximately 60° to σ_1 (Fig. 5i). At first wing cracks begin to develop on some but not all joints (Fig. 5ii). The orientation of the propagating wing cracks are similar to those predicted for isolated joint pairs in Fig. 3. As the simulation continues (Fig. 5iii–vi) several types of linkage structures are observed which are similar to those in Fig. 3; note that only six frames are shown from a simulation consisting of 350 steps. At Location A the linking structure is similar to that for an overlapping pair of joints in an extensional orientation. At Location B the structure is similar to that for under-lapping joints in a contractional geometry (the joints under-lap by a single mesh element). At Location C the

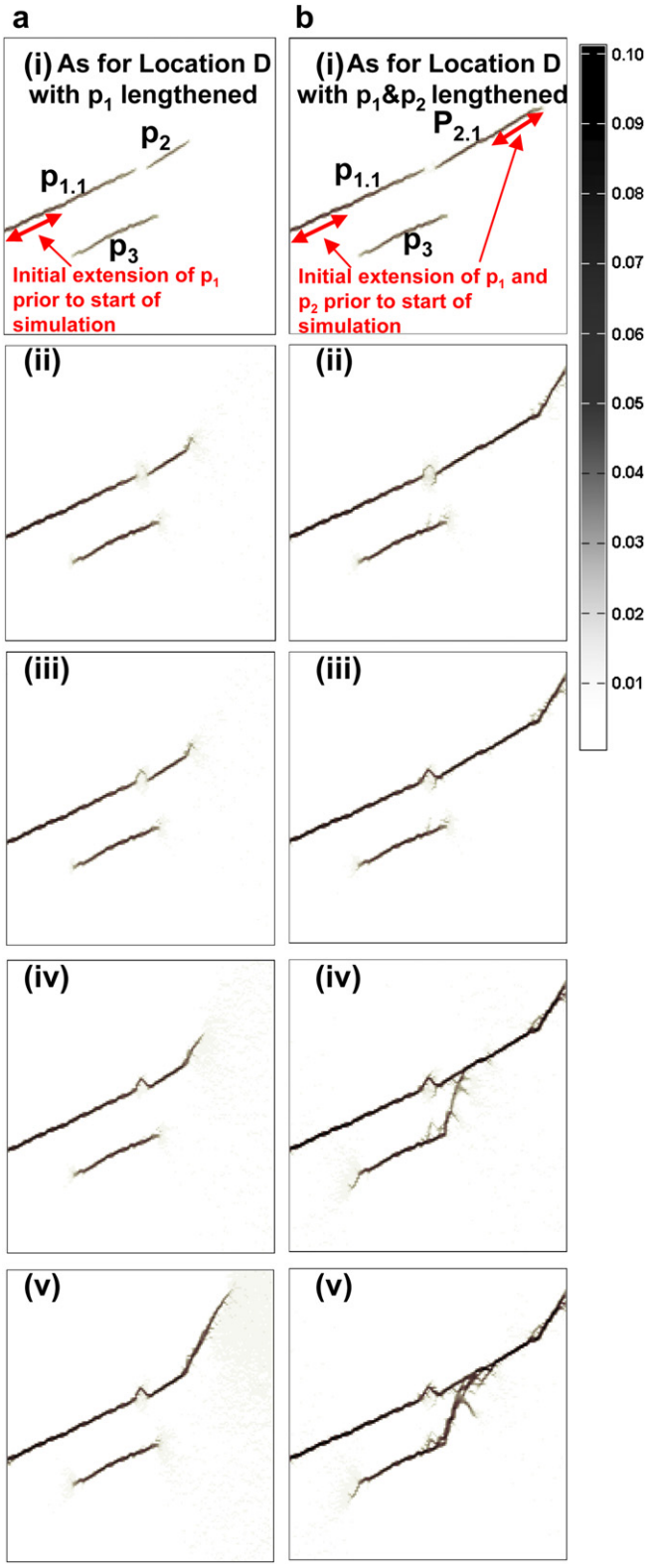

Fig. 10. Spatial and temporal evolution of strain predicted by MOPEDZ with pre-existing structures in the same relative positions as Location D but with (a) the initial length of p_1 doubled ($p_{1.1}$) and (b) initial length of p_1 and p_2 were both doubled ($p_{1.1}$ and $p_{1.2}$ respectively). Note that wing cracks only develop on p_3 when the upper wing cracks reach the boundary; had it not done so the growth of wing cracks from p_3 would have been suppressed. (All faults are left lateral.)

structure is the same as that for under-lapping joints in an extensional geometry. At Location D stepover geometries for both overlapping extensional joints and under-lapping contractional joints are represented, the predicted linkage structure is similar to that for overlapping joints in an extensional orientation.

At Location E the linkage structure that develops is different to that predicted for an isolated pair of under-lapping contractional joints (Fig. 3b); at E initial failure occurs in the host rock between the two joints as opposed to propagating from the joint tips. Because processing time for the large simulation (<20 joints) was 5–6 days, a small (6400 element mesh) simulation investigated local behaviour at Location E using three joints in the same relative positions; both the physical size represented by each finite-element and the boundary conditions (progressive displacement of the σ_1 boundaries starting from an initial value of $\sigma_1 = 2\sigma_3$) remain the same as that for the large simulation in Fig. 5. The stress field (Fig. 6a) shows that the relative positions of the pre-existing joints facilitates interaction of the compressional quadrants of the two joints (j_1 and j_3), which results in linkage due to shear failure. In the simulation joints j_1 and j_3 shown in Fig. 6b overlap by 38 mm. If the tip of joint j_3 is adjusted (by at least 38 mm either way) either to clearly over- or under-lap j_1, linkage geometries are similar to those expected for over- or under-lapping contractional joints (Fig. 3b; Fig. 12 in Segall and Pollard, 1980).

Three joints circled at Location A form two stepovers. The left stepover is extensional and the right stepover is contractional. The damage evolution (Fig. 7a) and strain evolution (Fig. 7b) in a small-scale simulation (6400 elements) with the joints in the same relative locations shows two types of linkage structure. Initially, the pair on the left behaves as the extensional geometry in Fig. 3c. However, as the fracture propagating from the middle of the upper joint lengthens, it begins to interact with the joint on the right of the figure, changing its orientation and eventually resulting in linkage of the pair of joints on the right that are in a contractional geometry (Fig. 3d).

Location B evolves a linkage structure similar to that predicted in Fig. 3b for under-lapping contractional geometries (the joints are displaced from being collinear by approximately 1 cm). At Location D, despite the upper two joints being closer together than those at Location B and in a more pronounced under-lapping contractional geometry, a similar linkage structure does not develop. Instead, a wing crack propagates from the much more distant, extensionally-related joint below. This geometry illustrates the effect of neighbouring joints, which is investigated by a small-scale simulation of the three joints at Location D. The initial joint configuration is shown in Fig. 8a and the magnitude of σ_1 prior to failure is shown in Fig. 8b. Comparison of Fig. 8b with the stress fields which are predicted for each of the three joints if simulated separately (Fig. 9) shows that having all three joints present reduces the magnitude and extent of the region of compressional stress surrounding the interacting tips, and increases the magnitude and extent of the tensional stress, most notably between joints p_2 and p_3. This explains the linkage structure that develops between the more distant extensional pair of joints, evident from the strain evolution (Fig. 8c). The resulting fracture pattern is similar to that seen in a geometrically similar configuration of starter joints in Segall and Pollard (1980, their Fig. 12).

3.1.1. *The influence of joint length on linkage*

The extent of the local stress perturbation associated with a fault has previously been related to its trace length (e.g. Segall and Pollard, 1980). To explore the effect of joint length on evolving fault linkage, small-scale simulations were performed adjusting the joint configuration at Location D. The lengths of the upper

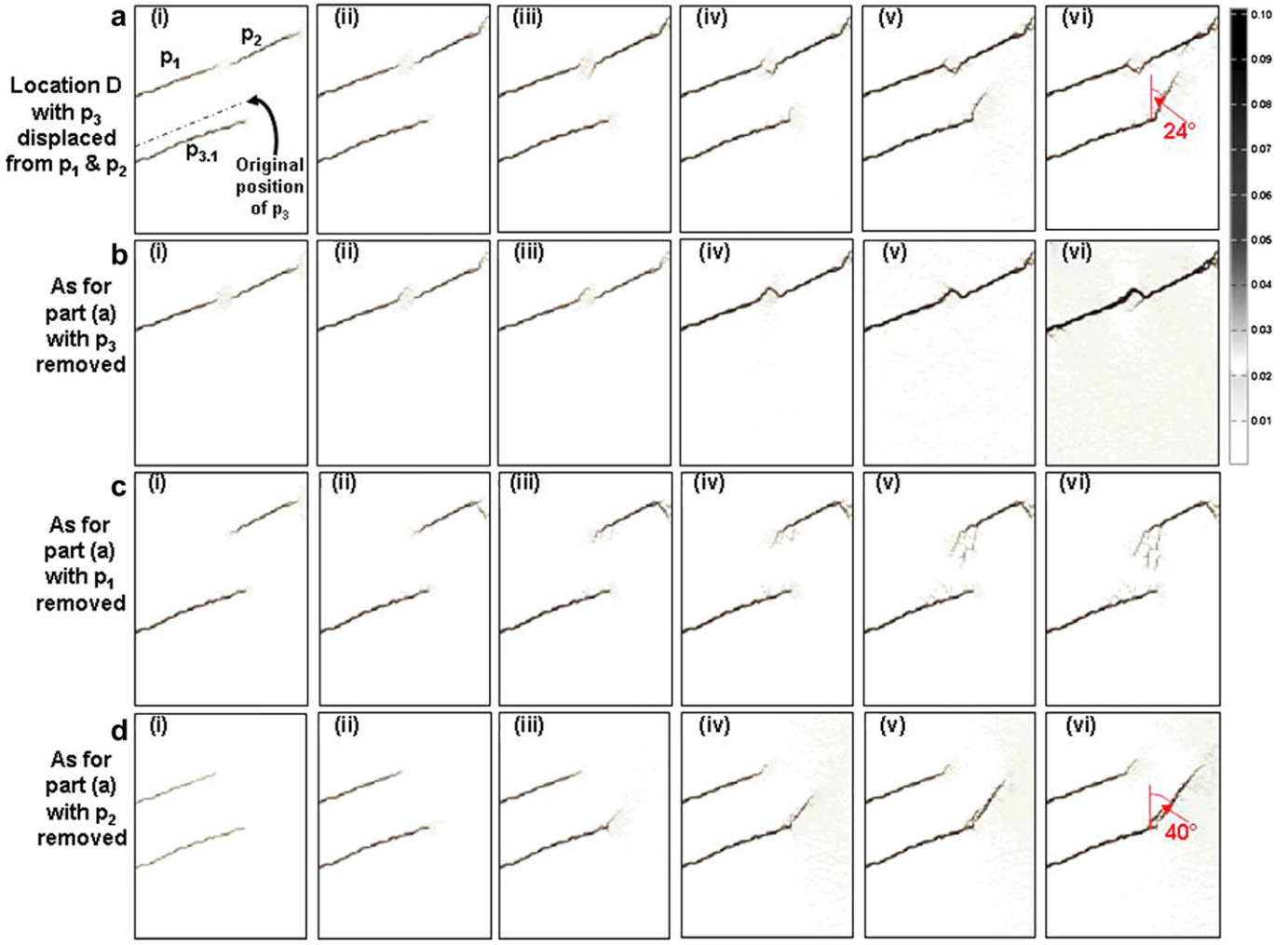

Fig. 11. (a) Spatial and temporal evolution of strain predicted by MOPEDZ with joints in the same relative positions as Location D but with p_3 displaced away from the upper two joints. Temporal evolution of strain predicted by MOPEDZ (b) if p_3 is removed, (c) if p_1 is removed and (d) if p_2 is removed. Note that the angle of the wing crack propagating from the p_3 is 24° for simulation (a) but is 40° for simulation (d).

joints (p_1 and p_2) were increased, keeping the relative position of the adjacent joint tips constant (Fig. 10). When the length of either one (Fig. 10a) or both (Fig. 10b) of the upper joints are doubled, joints p_1 and p_2 link in a manner similar to that for under-lapping contractional joint pairs. Previously, in Fig. 8, linkage was between the extensional pair of joints p_2 and p_3. From these simulations it is apparent that the length of the joints affects the magnitude and extent of the stress field at the joint tips, thus enhancing or decreasing the likelihood of linkage between a pair of joints.

3.1.2. Separation between joints

Small-scale simulations consisting of up to three joints were used to explore the effect of joint separation; this was investigated by increasing the distance between joints in the y direction. The position of the lower joint (based on the configuration at Location D) was adjusted until it was separated enough to allow the upper two (p_1 and p_2) to link (Fig. 11a). The stress perturbations due to each joint were then explored by systematically removing each from the simulation (leaving only two joints in the simulation). This produced varying joint linkage geometries from joints linking rapidly (Fig. 11b) through joints that fail to link, but show an evolving structure within the linkage zone (Fig. 11c) to joints which do not link (Fig. 11d). Note that in this final simulation (Fig. 11d) the wing crack which develops from p_3 does so at a different angle (40° from σ_1) than for the original simulation (24° from σ_1). Simulations illustrated in Fig. 11 show that the proximity of neighbouring joints affects both the location and orientation of the linkage structures that develop.

3.2. Exploring the effect of orientation of the regional stress field

Simulations of linkage from isolated pairs of joints in Lunn et al. (2008) showed that one of the key factors controlling the fault-zone geometry was the orientation of the joints to σ_1. In the case of joints at a low angle to σ_1 wing cracks were found to propagate back into the compressional quadrant, similar to structures observed in the field (Vermilye and Scholz, 1998). To explore what effect the orientation of σ_1 can have on fault-zone evolution from a complex joint pattern, the joints in Fig. 4 were oriented at an angle of approximately 30° to σ_1 (Fig. 12i). The predicted evolution of linkage structures through time is shown in Figs. 12ii–vi; a visual comparison of Fig. 12vi and Fig. 5vi shows the final geometries to be very different. Critically, joint traces that were approximately co-linear now progressively link up along strike to form long smooth linear fault traces (e.g. Locations

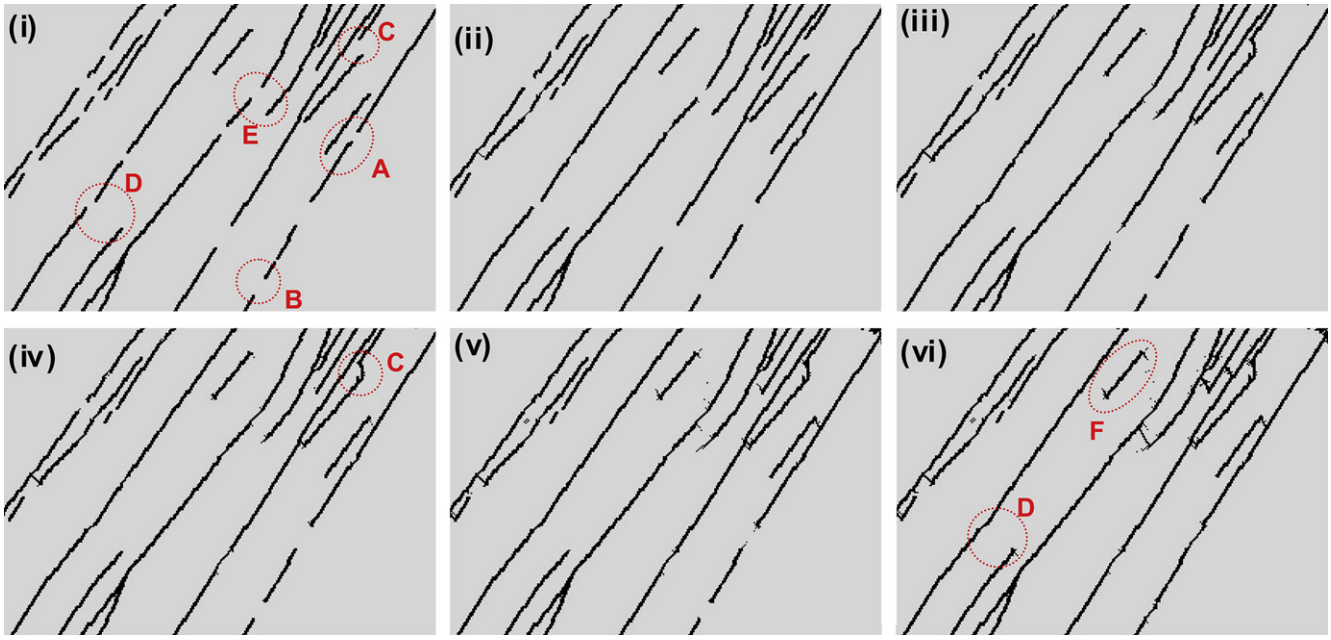

Fig. 12. Damage plot showing six frames from a simulation consisting of 350 steps which show the spatial and temporal evolution of the fractures predicted by MOPEDZ from (i) the initial joint pattern through to (vi) the final structure. The joints are oriented at 30° to σ1. Locations A–E indicated on (i) correspond to those in Fig. 5i. Simulation was carried out with the same initial conditions as that shown in Fig. 5. All faults are left lateral.

B and D). Further, the few wing cracks that do evolve in Fig. 12 only develop once neighbouring joints have linked to form through-going faults and propagate back into the compressional quadrant (e.g. Locations A and F). The only exception to this is at Location C, (Fig. 12iv) where an extensional stepover of the under-lapping joints develops.

The alteration of σ_1^{LOCAL} and σ_3^{LOCAL} in both magnitude and direction at the tips of a propagating fracture (or the original joint) results from a combination of factors (Fig. 13).

- The shape of the stress field around a fracture or joint is affected by its orientation with respect to the simulated far-field stresses σ_1 and σ_3 (Fig. 13a).
- The stress fields of neighbouring faults and/or fractures interact such that they can act to enhance or diminish local perturbations in the stress field (Fig. 13b).
- Wing cracks which have a different orientation to that of the initial joint will generate new perturbations in the local stress field (Fig. 13b(ii) for 60°).

These factors that control the perturbations in the local stress field have an influence on the different styles of linkage structures which develop between initially co-linear joints.

Three key observations are apparent from a comparison of the simulation results for pre-existing joints at 60° and 30° to σ_1:

- For the simulation at 60° to σ_1 (Fig. 5), the linking wing cracks are at a much wider variety of angles (e.g. see Locations B and D in Fig. 5) than those at 30° to σ_1 (Fig. 12).
- For the simulation at 60° to σ_1 (Fig. 5) many joints develop multiple wing cracks at individual joint tips and linkage structures tend to exhibit more damage than those at 30° to σ_1 (e.g. compare Location D in Figs. 5 and 12).
- With structures at 30° to σ_1, approximately 60% of the joints link along strike forming smooth linear features which span the model domain (Fig. 12); these features do not form for the simulations at 60° to σ_1,

4. Discussion

The simulations show three key findings: (1) local spatial and temporal variations in the stress field have a significant effect on the location, orientation and timing of wing crack development, resulting in significantly different patterns than those predicted from consideration of single fractures or pairs of fractures. (2) A significant difference in resulting fault-zone geometry is predicted when σ_1 is oriented at 30° with respect to the initial joint pattern (Figs. 5 and 12). (3) The spatial distribution (lengths, separation, overlap, under-lap, spacing) of the original joints is a key control on the predicted locations, orientations and timing of wing crack development.

4.1. Local variations in the stress field

The simulations focus on fault formation via linkage of pre-existing original joints and show that the proximity of neighbouring joints, and their effect on the local stress field, affects both the location and orientation of the linkage structures that develop. The large-scale simulations represent an area approximately 4.5 m wide interestingly, similar results are predicted if the model domain represents a larger physical size (e.g. several kilometres wide), where the initial features are 20 en-echelon pre-existing faults (the only difference being the physical size represented by each element in the finite-element mesh and the load required to create the same number of damaged elements).

Currently researchers in many fields use predictions of static stress distribution around an existing fault network to predict the locations and orientations of likely fracture zones (Maerten et al., 2002; Micklethwaite and Cox, 2004). Our simulations demonstrate that the locations of active fracture zones associated with faulting are likely to be critically affected by the constantly evolving local stress field as the fracture network develops. Simulations suggest that, in some cases, fracture zones will not begin to develop until adjacent through-going faults have fully formed. Further, the orientations of these fractures will be influenced by the evolving

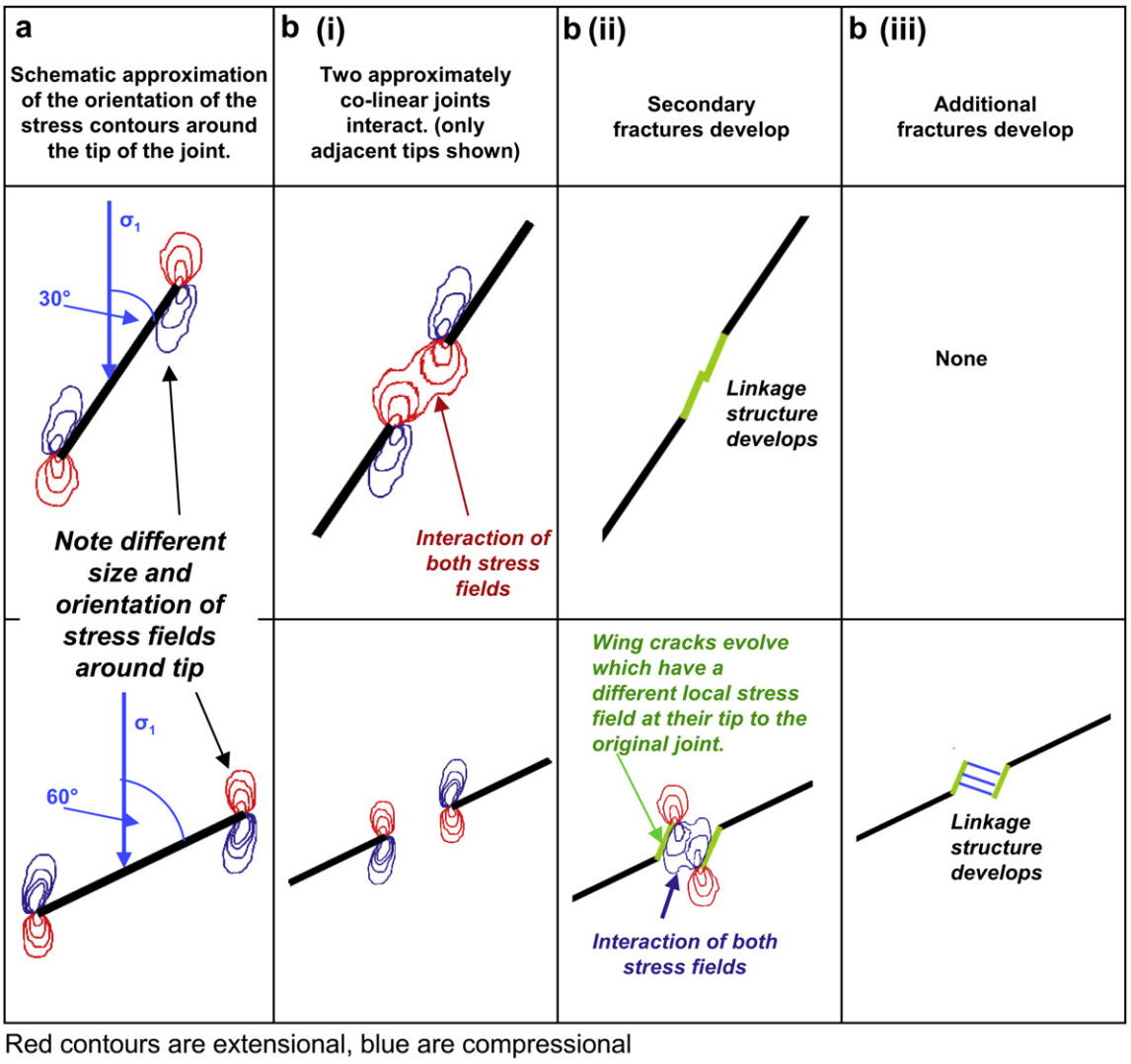

Fig. 13. Smoothed stress contours around the tip of a joint (or fault). (a) Orientation of the joint to the far-field stress affects the orientation of the local stress field around the tip (red contours are extensional stress contours, blue are compressional stress contours). (b) Different styles of linkage structures which develop between initially co-linear joints due to different interaction of the local stress field. Here joints at 30° to σ_1 link up approximately along strike, those at 60° develop wing cracks which later link through additional fracturing when the local stress field associated with the wing cracks interact. (For interpretation of the references to colour in this figure legend, the reader is referred to the web version of this article.)

geometry and proximity of neighbouring features within the network. Hence, predictions of the location and orientation of fracture zones, such as those by Maerten et al. (2002) and Micklethwaite and Cox (2004) may be improved by incorporating simulation of the constantly evolving local stress.

4.2. Orientation of the maximum compressive far-field stress

For a simulated σ_1 at a high angle to the original joints (Fig. 5), faults are principally formed by slip on pre-existing joints which then grow in length as wing cracks evolve and link originally discontinuous adjacent fault traces, resulting in a 'stepped' fault-zone geometry. A comparison of these results with Fig. 1 shows them to be similar to the complex fault-zone geometry in Fig. 1b (Martel, 1990); a large number of wing cracks and linkage structures are present, at a variety of angles, with few through-going features. Our simulations suggest that the faults from the Waterfall region of the Sierra Nevada (Fig. 1b) were formed under σ_1 at approximately 60° to the original joints. This angle to σ_1 differs from the 25°–30° derived for the same field site using linear elastic fracture mechanics (LEFM) by Segall and Pollard (1983) and Martel (1997); this may be due to the assumptions inherent in LEFM where failure is inferred from the steady-state stress distribution local to a single infinitely thin fracture within an infinite elastic domain.

For σ_1 at a low angle (30°) to the original joints, smooth linear faults are predicted by the simulations with a small number of linking fractures propagating back into the compressional quadrant. A comparison of Fig. 12 with the field observations shows the predicted fault geometry to be similar to that in Fig. 1a (Pennacchioni and Mancktelow, 2007) for the small NE-striking faults (these are labelled as fractures but offset the aplite). We suggest that these NE-striking faults may have formed by linkage of small joints and fractures when σ_1 was oriented approximately NNE.

Smooth co-linear fault traces such as those in Fig. 1a are commonly observed in field exposures. However, they are not generally interpreted from field data as having evolved from linkage of co-linear joint traces, but instead are mapped as long, small offset faults. In many cases this is likely to be because it is difficult from field data alone to distinguish whether individual

along strike sections of a fault originated as co-linear joints or formed through along strike linkage. Multiple offset markers could be useful because sites of linkage commonly remain as displacement minima along a fault that develops by segment linkage (e.g. Bürgmann et al., 1994). However, the aplite dykes used as offset markers are rare in both of the field areas in Fig. 1. It is possible that the fault gouge within a slipped joint will have a different mineralogy, grain size distribution or fabric than that along a linkage fracture.

The faults from the Bear Creek region of the Sierra Nevada (Fig. 1c) are a combination of frequent through-going 'smooth faults' and multiple wing cracks (typical of more 'stepped' fault-zones). We suggest that at this location one or more rotations of σ_1 may have occurred during fault-zone evolution as discussed by Segall and Pollard (1983). Rotation of σ_1 may be caused by an actual change in the regional stress field or by more local evolution of the stress field during development of larger scale structures (e.g. due to nearby linkage of faults at a scale one order of magnitude greater than those simulated here).

5. Summary and conclusions

This paper applies a finite-element model, MOPEDZ, to investigate fault-zone evolution from more than 20 pre-existing joints in granite. We simulate fault-zone evolution for maximum compressive far-field stress (σ_1) at 30° and 60° to the orientation of the pre-existing joints. Key findings from the simulations are:

(1) Local spatial and temporal variations in the stress field arise from interactions between neighbouring joints that have a significant effect on the predicted locations, orientations and timings of wing crack development.
(2) A clear difference in fault-zone geometry is predicted depending on the orientation of σ_1 with respect to the initial joint pattern: for σ_1 at an angle of 30° to the initial joints, co-planar joints progressively link up along strike to form long 'smooth' linear faults with few additional wing cracks; for an orientation of σ_1 of 60° to the initial joints, a more fractured complex 'stepped' fault-zone geometry evolves with multiple wing cracks forming linkage structures at a variety of angles. Existing field data show that both 'smooth' and 'stepped' fault-zone trace geometries are commonly observed in crystalline rocks.
(3) Local spatial and temporal stress perturbations affect predictions of zones of enhanced fracturing within fault networks at larger scales.

Acknowledgements

Heather Moir is supported by a University of Strathclyde Faculty of Engineering scholarship. James Kirkpatrick is supported by the Natural Environment Research Council (NE/E005365/1). Insightful and thorough reviews by Steve Martel and Michael Gross and personal conversations with Steve Martel have significantly improved the manuscript.

References

Bergbauer, S., Martel, S.J., 1999. Formation of joints in cooling plutons. Journal of Structural Geology 21, 821–835.
Bremaecker, D.J.C., Ferris, M.C., 2004. Numerical models of shear fracture propagation. Engineering Fracture Mechanics 71, 2161–2178.
Bürgmann, R., Pollard, D.D., Martel, S.J., 1994. Slip distributions on faults: effects of stress gradients, inelastic deformation, heterogeneous host-rock stiffness, and fault interaction. Journal of Structural Geology 16, 1675–1690.
Byerlee, J.D., 1967. Frictional characteristics of granite under high confining pressure. Journal of Geophysical Research 72, 3639–3648.
Crider, J.G., Peacock, D.C.P., 2004. Initiation of brittle faults in the upper crust: a review of field observations. Journal of Structural Geology 26, 691–707.
Cruikshank, K.M., Aydin, A., 1994. Role of fracture localization in arch formation at Arches National Park, Utah. Geological Society of America Bulletin 106, 879–891.
Du, Y.J., Aydin, A., 1995. Shear fracture patterns and connectivity at geometric complexities along strike-slip faults. Journal of Geophysical Research-Solid Earth 100 (B9), 18093–18102.
Evans, J.P., Shipton, Z.K., Pachell, M.A., Lim, S.J., Robeson, K.R., 2000. The structure and composition of exhumed faults, and their implications for seismic processes. In: Bokelmann, G., Kovach, R.L. (Eds.), Proceedings of the 3rd Conference on Tectonic Problems of the San Andreas Fault System, vol. 21. Stanford University Publications, Geological Sciences, pp. 67–81.
Granier, T., 1985. Origin, damping and pattern of development of faults in granite. Tectonics 4, 721–737.
Jing, L., 2003. A review of techniques, advances and outstanding issues in numerical modelling for rock mechanics and rock engineering. International Journal of Rock Mechanics & Mining Sciences 40, 283–353.
Joussineau, G., Mutlu, O., Aydin, A., Pollard, D.D., 2007. Characterization of strike-slip fault-splay relationships in sandstone. Journal of Structural Geology 29, 1831–1842.
Kattenhorn, S.A., Marshall, S.T., 2006. Fault-induced perturbed stress fields and associated tensile and compressive deformation at fault tips in the ice shell of Europa: implications for fault mechanics. Journal of Structural Geology 28, 2204–2221.
Kattenhorn, S.A., Aydin, A.A., Pollard, D.D., 2000. Joints at high angles to normal fault strike: an explanation using 3-D numerical models of fault-perturbed stress fields. Journal of structural Geology 22, 1–23.
Kim, Y.J., Peacock, D.C.P., Sanderson, D.J., 2004. Fault damage zones. Journal of Structural Geology 26, 503–517.
Kirkpatrick, J.D., Shipton, Z.K., Evans, J.P., Micklethwaite, S., Lim, S.J., McKillop, P., 2008. Strike-slip fault terminations at seismogenic depths: the structure and kinematics of the Glacier Lakes fault, Sierra Nevada United States. Journal of Geophysical Research, B04304. doi:10.1029/2007jb005311.
Lunn, R.J., Willson, J.P., Shipton, Z.K., Moir, H., 2008. Simulating brittle fault growth from linkage of preexisting structures. Journal of Geophysical Research 113, B07403. doi:10.1029/2007JB005388.
Maerten, L., Gillespie, P., Pollard, D.D., 2002. Effects of local stress perturbation on secondary fault development. Journal of Structural Geology 24, 145–153.
Martel, S.J., 1990. Formation of compound strike-slip fault zones, Mount Abbot Quadrangle, California. Journal of Structural Geology 12, 869–882.
Martel, S.J., 1997. Effects of cohesive zones on small faults and implications for secondary fracturing and fault trace geometry. Journal of Structural Geology 19, 835–847.
Martel, S.J., Boger, W.A., 1998. Geometry and mechanics of secondary fracturing around small three-dimensional faults in granitic rock. Journal of Geophysical Research 103 (B9), 21299–21314.
Martel, S.J., Pollard, D.D., Segall, P., 1988. Development of simple fault zones in granitic rock, Mount Abbot quadrangle, Sierra Nevada, California. Geological Society of America Bulletin 100, 1451–1465.
Martin, C.D., 1997. Seventeenth Canadian geotechnical colloquium: the effect of cohesion loss and stress path on brittle rock strength. Canadian Geotechnical Journal 34, 698–725.
Mathews, J.H., Fink, K.D., 2004. Numerical Methods using Matlab, fourth ed. Pearson Prentice Hall, New Jersey.
Micklethwaite, S., Cox, S.F., 2004. Fault-segment rupture, aftershock-zone fluid flow and mineralization. Geology 32, 813–816.
Myers, R., Aydin, A., 2004. The evolution of faults formed by shearing across joint zones in sandstone. Journal of Structural Geology 26, 947–966.
Pachell, M.A., Evans, J.P., 2002. Growth, linkage, and termination processes of a 10-km-long strike-slip fault in jointed granite: the Gemini fault zone, Sierra Nevada, California. Journal of Structural Geology 24, 1903–1924.
Pachell, M.A., Evans, J.P., Taylor, W.L., 2003. Kilometer-scale kinking of crystalline rocks in a transpressive convergent setting, Central Sierra Nevada, California. GSA Bulletin 115, 817–831.
Peacock, D.C.P., Sanderson, D.J., 1995. Strike-slip relay ramps. Journal of Structural Geology 17, 1351–1360.
Pennacchioni, G., Mancktelow, N.S., 2007. Nucleation and initial growth of a shear zone network within compositionally and structurally heterogeneous granitoids under amphibolite facies conditions. Journal of Structural Geology 29, 1757–1780.
Segall, P., Pollard, D.D., 1980. Mechanics of discontinuous faults. Journal of Geophysical Research 85, 4337–4350.
Segall, P., Pollard, D.D., 1983. Nucleation and growth of strike slip faults in granite. Journal of Geophysical Research 88, 555–568.
Shen, B., Stephansson, O., 1993. Numerical-analysis of mixed mode-I and mMode-II fracture propagation. International Journal of Rock Mechanics and Mining Sciences 30, 861–867.
Tang, C.A., 1997. Numerical simulation of progressive rock failure and associated seismicity. International Journal of Rock Mechanics and Mining Sciences 34, 249–261.
Turcotte, D., Schubert, J., 2002. Geodynamics, seconnd ed. Cambridge University Press, Cambridge.
Vermilye, J.M., Scholz, C.H., 1998. The process zone: a microstructural view of fault growth. Journal of Geophysical Research 103, 12223–12237.
Willemse, E.J.M., Peacock, D.C.P., Aydin, A., 1997. Nucleation and growth of strike-slip faults in limestones from Somerset, U.K. Journal of Structural Geology 19, 1461–1477.
Willson, J.P., Lunn, R.J., Shipton, Z.K., 2007. Simulating spatial and temporal evolution of multiple wing cracks around faults in crystalline basement rocks. Journal of Geophysical Research-Solid Earth 113, B07403. doi:10.1029/2007JB005388.